ICPC 2019 – 2.3

Development and testing of an innovative gas engine for heavy duty applications

Stefano Golini, David D'amato, Sergio Giordana, Paolo, Grosso, Diego Iudice
FPT Industrial

Anton Arnberger, Gernot Hasenbichler
AVL List GmbH

Davide PAREDI
Politecnico di Milano

Peter Grabner
TUG

ABSTRACT

The need to drastically reduce GHG emission in the next decade will deeply change the technological solutions employed for long haul transportation. Several alternatives are possible and, among them, natural gas engines have proved a reliable and efficient way to curb GHG emission.

FPT Industrial is currently the European leader in the production of NG engines and joined the research project HDGAS (co-funded by the EU), aimed at the development of NG powertrains for the 2020s, to offer NG engines with increased fuel efficiency.

This paper describes the challenges encountered during the development of the HDGAS engine and presents results of the simulations and testing performed during the project.

INTRODUCTION

At the end of 2018 the European Council introduced limits on CO_2 emissions from HD vehicles: compared to the 2019 average, a reduction of 15% is foreseen in 2025, which will become 30% in 2030.

Compared to the uniformity of today's HD vehicles (100% ICEVs, diesel engines > 99%), in 10 to 20 years the landscape will be significantly more varied, because it will be impossible to meet these limits relying only on the development of the diesel engine. A revolution will take place in the next few decades, which will bring about different vehicles and fuels to move goods across the world.

Electrical vehicles seem to be the most probable candidate to replace ICEs in the near future. It must be underlined, though, that the battery efficiency decreases as the vehicle size increases **[1] [2]**: this means that BEVs could be a viable options for LCV but it will be more difficult for them to replace ICEs in LH applications. Furthermore, the technical principles for the electrification of trucks are similar to those available for cars but the greater size and weight of trucks and their more rugged operations substantially increase the barriers to batteries serving as a substitute for diesel engines **[2]**.

It must be underlined that the impact on the environment of this technology is not negligible: the LCA of BEVs shows that they have a global effect similar to traditional vehicles **[3]**: this is highly dependent on the way electricity is produced **[4]** and with the current European mix, in which renewable energy accounts only for 26% of the total **[5]**, the positive effect of BEVs on global warming is very limited **[1]**. In the current situation, BEVs can be effective in reducing the pollutants level in urban areas: this factor must not at all be underestimated but will have little or no effect in reducing GHG emission **[3]**.

In addition, batteries need raw materials, such as lithium and cobalt, whose production must be

increased substantially in order to meet the global demand of BEVs and there is a risk that large scale exploitation of these resources could lead to significant environmental impacts **[4]**. What's more, the effect on water reserves must in no way be overlooked.

Fuel cells are another candidate foreseen to replace the ICE, at least partially, on LH missions. An FCV is, essentially an electric vehicle using hydrogen stored in a pressurized tank and equipped with a fuel cell for on-board power generation. Hydrogen is stored on vehicles in dedicated tanks at pressures of 35 MPa to 70 MPa: the energy density is much higher compared to batteries, but hydrogen storage still needs four times more space to achieve the same range as conventional diesel technology **[2]**.

Today, around 50% of hydrogen is produced from natural gas through steam methane reforming, and one-third comes from the refining process of oil; the rest is produced from either coal or electrolysis **[2]**. From this, it follows that the ideal pathway for hydrogen production is electrolysis, using renewable energy. Alternatively, biomethane and the use of carbon capture and storage also provide another way to generate hydrogen with low life cycle GHG emissions **[2]**.

Currently, there around 500 FCVs (mainly cars and buses) running across several demonstration projects globally, but the interest in hydrogen and FCVs is growing: up to 400 stations are planned to be operating in Germany by 2023 while California has set the goal of having 100 stations by 2020 and has developed funding programmes to achieve this target **[2]**. Nevertheless, it must be considered that the time needed to bring hydrogen-refuelling stations online is significant (California estimates it at two years **[6]**) and that refuelling is, in any case, a very complex operation, especially when using 70 MPa.

The high cost of the main components is another barrier that must be overcome. Current cost of FCs is around 1000$/kW and it will be necessary to wait for high-volume manufacturing of next generation of FCs to bring the cost somewhere between 60 and 200 $/kW **[2]**. The tank is another very expensive item, ranging from 40 to 60 $/kWh (at 70 MPa): a storage tank of 1400 kWh, that should guarantee a 700-km range, will then stay between 56000 and 84000 $. Costs are expected to fall to 15-30 $/kWh, though at a slower pace compared to FCs **[2]**.

The time necessary to build the infrastructure for the new vehicles, be they BEVs or FCVs, is a factor that must be fully accounted for, as more than few years will be necessary to put in operation the over 25000 charging points (20000 DC 150-500 kW and > 5000 DC >500 kW, along motorways) and the 1000 hydrogen refueling stations (500 for compressed H_2 and 500 for liquefied H_2) that are estimated as necessary by 2025-2030 to meet the EU standards on CO_2 **[7]**.

In the meanwhile, decarbonisation will have to be pursued reducing ICE's GHG emission and this can be accomplished reducing the carbon content of the fuel: natural gas (a blend of different hydrocarbons, mainly methane) is the immediate replacement for diesel fuel.

To begin with, combustion of NG produces the lowest CO_2 quantity per unit of energy of all other hydrocarbons **[8]**: due to the fact that NG has the lowest C/H ratio and the highest energy content per unit of mass, its combustion generates 58.5 gCO_2/MJ versus 78 gCO_2/MJ for diesel fuel, a reduction around 25%, assuming the same thermal efficiency. The higher efficiency of the diesel engine lessens this amount, but it remains still significant: a recent study **[9]** showed that, on a well-to-wheel basis, a HD NGV using CNG will produce 16% less CO_2 than the corresponding diesel vehicle.

Moreover, NG can be obtained totally from renewable sources: the number of biomethane plants in the EU rose from 180 in 2011 to 420 in 2015 **[2]** and biomethane is obtained from agricultural residuals or from landfills, so it is not in competition with food. If NG is obtained from renewable sources, GHG emission will be, on the average, 23% of GHG emission with fossil NG **[9]**.

Since NG technology has been around for the past few decades, the distribution network is well established and it is continuously growing (**Figure 1**).

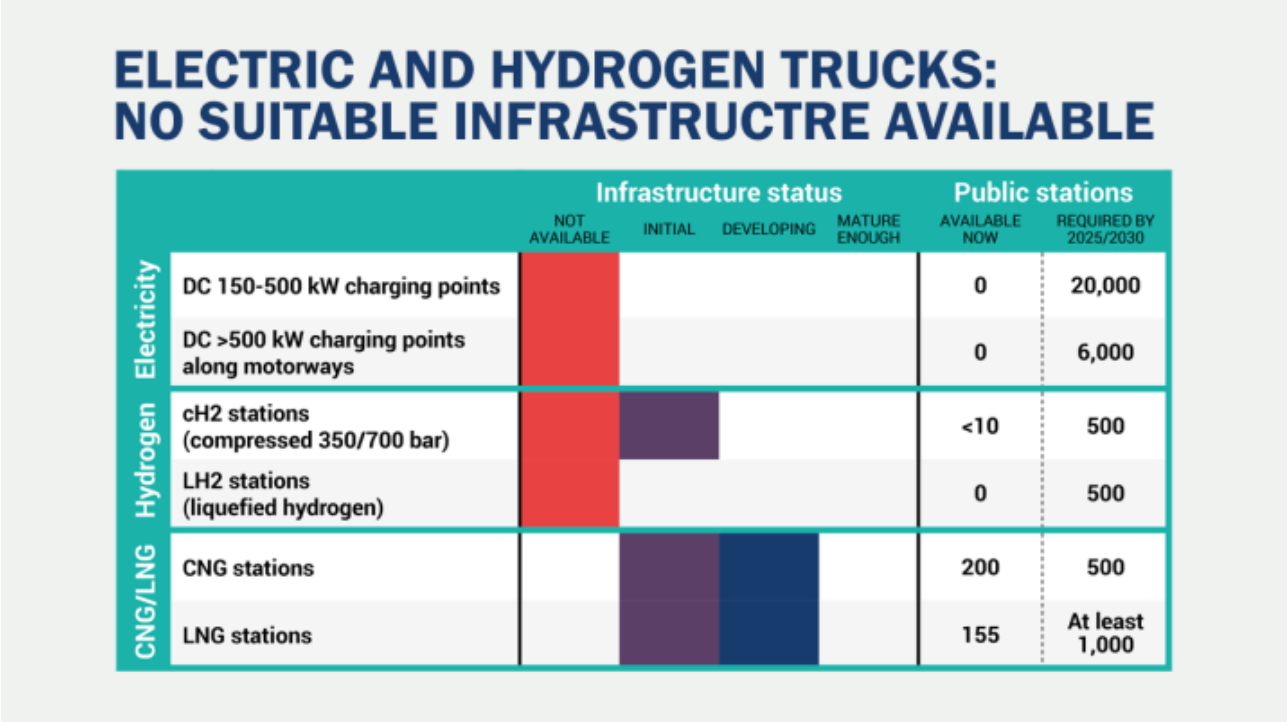

Figure 1 Infrastructure of “alternative fuels” for HDV [7]

NG HDVs have been available for the past twenty years and the most recent products, such as the IVECO Stralis NP460 (powered by FPT’s Cursor13 NG), can replace the correspondent diesel vehicle, both in terms of performance and in terms of range (more than 1600 km with two LNG tanks **[10]**). Furthermore, the use of NG can lead to important savings on the fuel cost: LNG price in China in the past decade has been, on the average, 55% of diesel fuel price, on an energy equivalent basis and the number of LNG lorries skyrocketed from 7000 in 2010 to 132000 in 2015 **[2]**. But also in Europe, NG is significantly cheaper than diesel fuel and can tip the overall economic balance in favour of the LNG vehicle **[10]**.

The already significant advantages of NGVs in terms of lower GHG emissions and lower operating cost can be improved by improving the efficiency of NG engines. FPT Industrial has developed NG engines since 1990s and strongly believes that this engine is one of the possible solutions (certainly the most readily available) to reduce the environmental impact of transportation.

In order to reach this target and to offer to its Customers more efficient and economically viable products, FPT Industrial joined the HDGAS project, aimed at developing innovative gas engines for the 2020s.

THE HDGAS PROJECT

The HDGAS project started in May 2015 and lasted 36 months. It was co-funded by the EU in the framework of HORIZON2020 and it involved 20 partners from 9 different countries across the EU, from both the academic and the industrial world.

Its goal was to develop, demonstrate and optimise advanced powertrain concepts for NG engines, to perform thereof integration into HD vehicles, and to confirm achievement of Euro VI emissions limits, and in use compliance under real-world driving conditions, while reducing CO_2 emissions at least 10% with respect to 2013 state-of-the-art engines.

Three different ICEs were developed in the project along with innovative after-treatment systems. Moreover, a new concept of LNG tank was pursued, in order to increase vehicles’ range. Finally, technical requirements and international/European standards for LNG fuelling interfaces were drawn.

Project Organization

In order to achieve the above-mentioned goals, the HDGAS project was organised in 8 work packages (WP), as shown in **Figure 2**Fehler! Verweisquelle konnte nicht gefunden werden.:

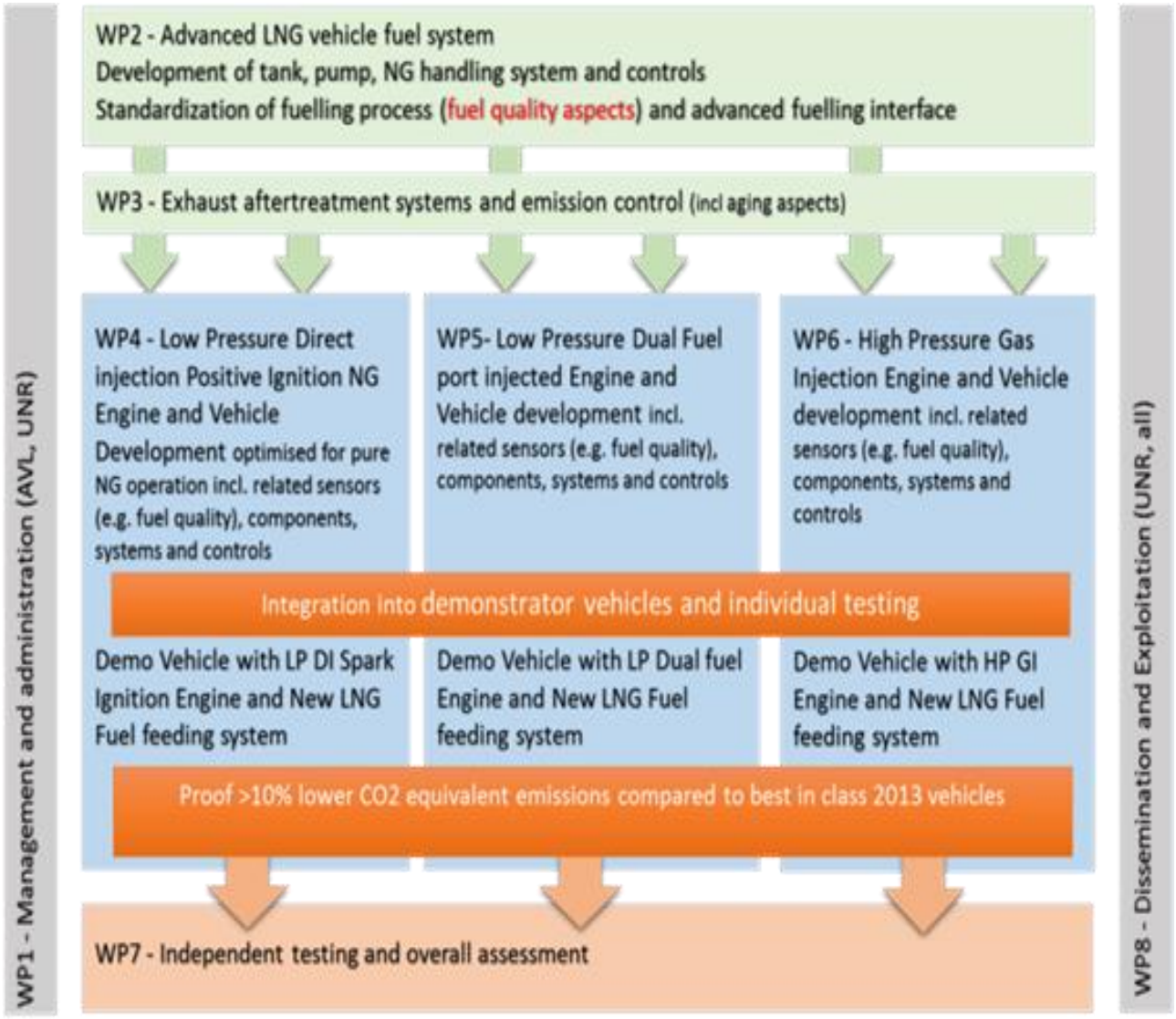

Figure 2 HDGAS structure

- WP1 (led by AVL and Uniresearch) to manage the Project
- WP2 (led by Daimler) aimed at the development of advanced tank systems as well as standardization of fuelling process and interface
- WP3 (led by Ricardo) aimed at the development and demonstration of a new generation of ATSs
- WP4 (led by FPT Industrial) aimed at the development of an innovative positive ignition NG engine
- WP5 (led by MAN) aimed at the development of a dual-fuel, port-injected engine
- WP6 (led by Volvo) aimed at the development of a high-pressure gas injection engine
- WP7 (led by AVL) to determine testing procedures and overall results assessment
- WP8 (led by Uniresearch) to disseminate Project's results.

Prof. Dr. Theodor Sams, from AVL Graz, was the Project Coordinator. Further information can be found at the Project's website (www.hdgas.eu).

In particular, WP4, led by FPT Industrial, was devoted to the development of an innovative positive-ignition engine exclusively fuelled by natural gas, and the integration of the engine in a long haul truck, along with the new LNG tank developed in WP2 and the innovative ATS developed in WP3.

Tests aimed at demonstrating the improved fuel efficiency were performed at test bench. The engine was tested in two different configurations, stoichiometric and lean burn, in order to evaluate potentialities in fuel consumption reduction of both but in this paper we will concentrate only on the stoichiometric version.

The target of -10% in GHG emissions and +10% in performance (torque/power) with respect to 2013 state-of-the-art engines was reached applying several new solutions to the HDGAS engine, such as:

- An innovative combustion system, with the intake ports and the combustion chamber specifically designed for combustion in spark-ignition engines, hence creating tumble rather than swirl
- A new fuel system, which makes it possible to employ different injection strategies in order to improve air/fuel mixing and, thus, combustion efficiency, reducing pollutant emissions at the same time
- Cooled EGR, to increase fuel efficiency
- High energy ignition system. With the Corona ignition system, the air/fuel mixture is ignited in a larger volume compared to a standard spark plug ignition system, so burn delay and burn duration can be significantly reduced, leading to a swifter combustion and improved late burn behaviour, reducing the risk of knock
- Variable Valve Timing, using a cam-phaser, on both the intake and the exhaust. Hydraulic valve lash adjustment was also employed
- Double overhead camshaft with inclined valves.

The high level of new content of this WP required the joint effort of several partners, each with a different role and task:

- FPT Industrial designed the new engine components and procured and built the prototype multi-cylinder engines. FPT also developed the stoichiometric configuration at test bench
- AVL tested the stoichiometric version on a single cylinder research engine
- IVECO integrated the HDGAS engine in the demonstrator vehicle, along with the new LNG tank and ATS
- BorgWarner supplied the high-energy Corona ignition system
- Politecnico di Milano performed CFD simulations of the stoichiometric configuration to assist the design of the combustion system
- Ricardo performed 1D and CFD simulations of the lean burn version and developed the same configuration at test bench
- Technische Universität Graz performed 1D simulations of the stoichiometric version to determine the best configuration of the engine in terms of subcomponents (EGR lay out, turbomachting, camshaft profile,…).

THE DESIGN PROCESS

It was clear from the beginning that the design of the HDGAS engine would have been a complex task, due to the features which required a totally new cylinder head as well as other fundamental components.

Some constraints were defined:

- First of all, the new cylinder head would have to be installed on the existing cylinder block, so the number and the position of the bolts as well the number and position of oil and water passages were fixed
- Secondly, the external dimensions of the new engine would have to be as close as possible to the Cursor13 NG engine, under development at the time
- Finally, the vehicular interfaces of the new engine would have to be the same (dimensions and position) of the aforementioned Cursor13 NG

The main characteristics of the engine are listed below.

Architecture	6-cylinder in line
Bore x Stroke	135 x 150 mm
Displacement	12.9 dm^3
Valves per cylinder	4
Camshaft lay-out	Double over-head
Valve drive	Finger follower

As we will see, the final configuration of the engine derived from a close cooperation between design and 1D and CFD calculations.

The Combustion System

The design of the combustion chamber is based on the pent roof concept, which has been proven to be the best configuration for spark-ignition engines, from the efficiency of combustion point of view **[12]**.

The design of the combustion chamber had to take into account the necessity to install the fuel injector and Corona ignitor, which are rather bulky objects: the two components were arranged in a configuration which allows good accessibility (for installation and maintenance) while keeping them as close as possible to the centre of the combustion chamber, to improve air/fuel mixing and to facilitate the mixture's ignition.

The final configuration of the combustion chamber is shown in **Figure 3**.

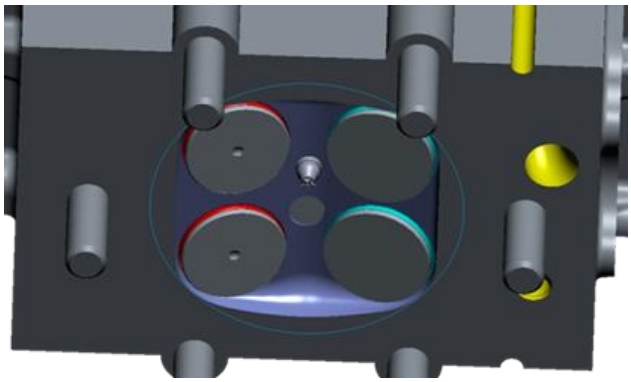

Figure 3 Combustion chamber

The intake ports were designed in order to reach the best values of tumble ratio and discharge coefficient: the latter is a measure of the turbulence level (beneficial for combustion propagation) in the combustion chamber, while the former quantifies the mass flow through the ports and into the cylinder.

The proposed design was checked with CFD, in order to find suitable values for both parameters. The discharge coefficient thus found was then fed into the 1D model in order to verify that it guaranteed a correct global behaviour of the engine.

As tumble ratio and discharge coefficients have opposite trend, the best trade-off was found after three iterations between design, CFD and 1D simulations: the final configuration is shown in **Figure 4** (see also **Figure 19**).

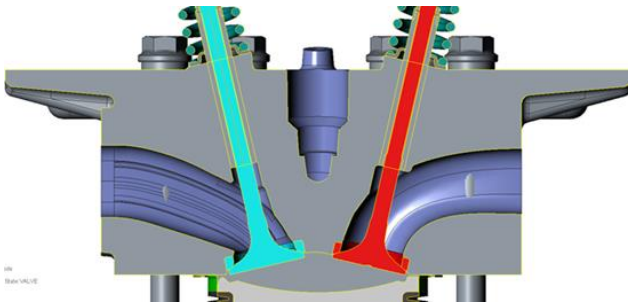

Figure 4 Final configuration of the intake ports

The piston head was shaped in a lenticular way, in order to reach the desired compression ratio and pockets are present on the piston ceiling to avoid interference with valves at TDC.

The Cylinder Head and Overhead

The cylinder head is the core component of the C13 HDGAS, and it incorporates all the new solutions introduced in this engine, namely:

- Pent roof combustion chamber
- Inclined valves
- Direct injection system
- Corona ignition system.

The experience gained by FPT in more than ten years of designing high-performance NG engines greatly helped with this cylinder head. Therefore, some components (both geometry and material of valves and valve seats) and the cylinder head material are the same successfully used in other Cursor NG engines. The cylinder head material is a cast iron variant, particularly suitable for high temperatures found in stoichiometric combustion.

Figure 5 Cylinder head

FEA of the cylinder head, conducted according to FPT's standard practice, showed that the component can successfully withstand the thermal and mechanical loads expected during its mission.

The cylinder overhead is a large aluminum component which has multiple functions:

1. It houses the camshafts and the HVA
2. It serves as the cylinder head cover
3. It has a central, oil-free to room where the upper parts of the ignitors and of the injectors, and their electrical connectors, are located. The injection rail is also located here
4. It has an integrated rear pocket to accommodate chain drive, cam phaser and variable force solenoid.

The axial dimension of the camshaft journals has been kept to a minimum, in order to reduce friction. Moreover, the use of HVA eliminates the need for valve lash adjustment, thus reducing maintenance.

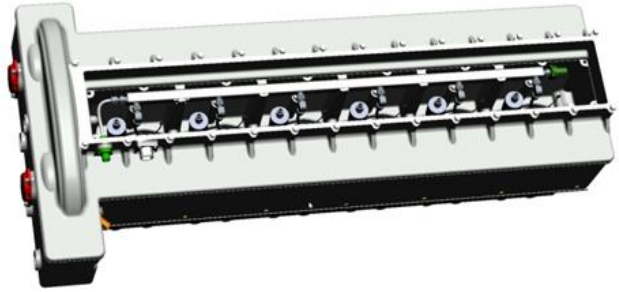

Figure 6 Cylinder overhead

Gear Train and Back End

The back end of the engine was also deeply modified, as this is the first Cursor engine to employ a double camshaft. Because of this, the gear train currently used on the Cursor13 engine was revised and it is still used in the lower part, close to the crankshaft, while a chain is used in the upper part to drive the two camshafts.

The flywheel housing was completely redesigned to house the new components.

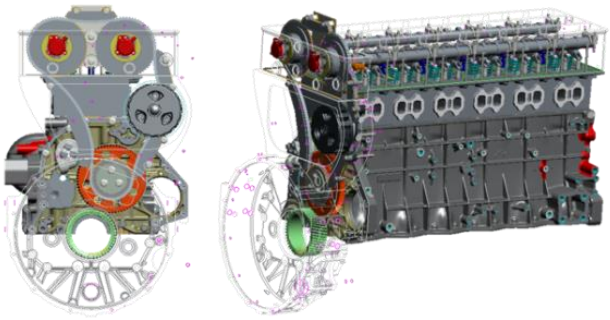

Figure 7 Back end

Intake Manifold

The intake manifold consists of two elements joined together: the fresh air-EGR mixer and the plenum.

In the mixer, fresh air enters through the throttle valve, coming from the charge air cooler, while EGR is added by the EGR nozzle, after it has passed through the cooler and its valve. The position of the EGR nozzle was determined with the aid of CFD calculation to obtain the optimal mixing between EGR and fresh air.

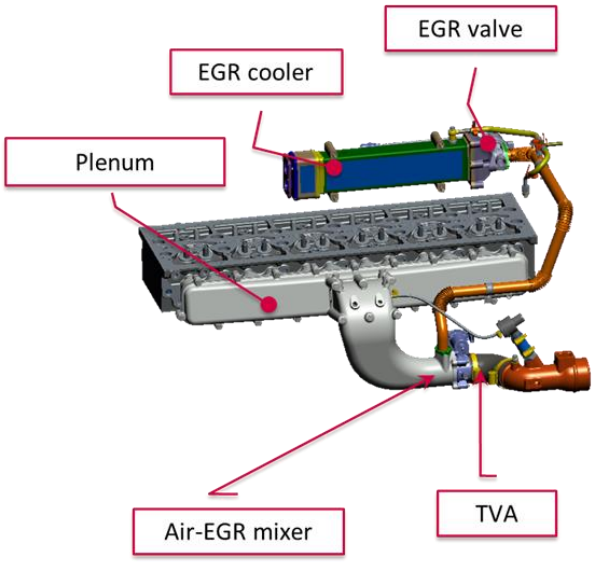

Figure 8 Intake manifold and EGR circuit

The plenum is connected to the cylinder head by means of 12 straight ducts, designed in order to reduce pressure losses to a minimum and to keep charge flow into the various cylinder as uniform as possible.

Exhaust Manifold and EGR Circuit

The EGR circuit is used to recirculate exhaust gas to the intake of the engine in order to reduce gas temperature during combustion, thus lowering NO_x production, wall-heat losses and sensitivity to knock; moreover, EGR reduces pumping losses in part-load operation **[12]**.

As it is customary with 6-cylinder engines, the turbocharger has a twin scroll, to avoid interference between pressure pulsations of the various cylinders. Therefore, it was decided to extract the EGR from both branches of the exhaust manifold. For the same reason, the turbocharger is equipped with two WGs, one for each turbine scroll: this configuration improves the engine efficiency, keeping both sections of the engines (i.e. cylinders 1 to 3 and cylinders 4 to 6) in the same conditions

The EGR routes are separated down to the EGR cooler and they are joined together only upstream the EGR control valve; reed valves are used to eliminate pressure fluctuations.

The FEA of the exhaust manifold showed positive results for this component too.

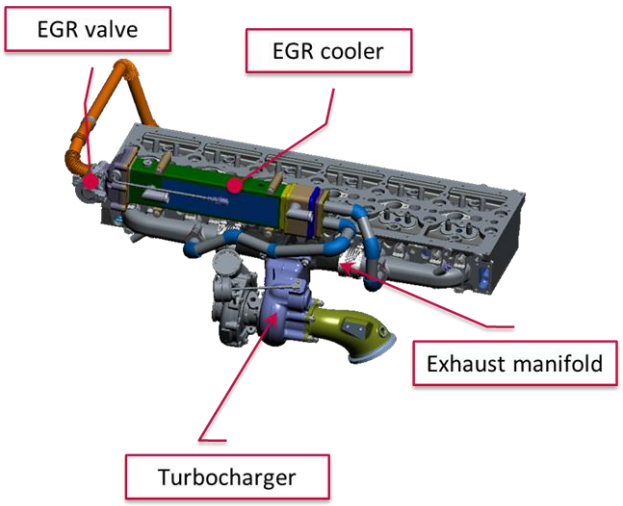

Figure 9 Exhaust manifold, TC and EGR cooler

External Packaging

The external shape and dimensions of the Cursor13 HDGAS engine were kept as much as possible similar to the current Cursor13 engine. Most interfaces are in the same position as those of the Cursor13 (intake duct upstream of the throttle valve,

turbine and compressor outlets) and the lay-out of the external components (turbocharger and exhaust manifold, EGR cooler and circuit) was designed in order to avoid interferences with the vehicle.

The result is a compact and elegant engine which can easily fit in the IVECO Stralis frame.

Figure 10 Cursor13 HDGAS engine

THERMODYNAMIC ANALYSIS

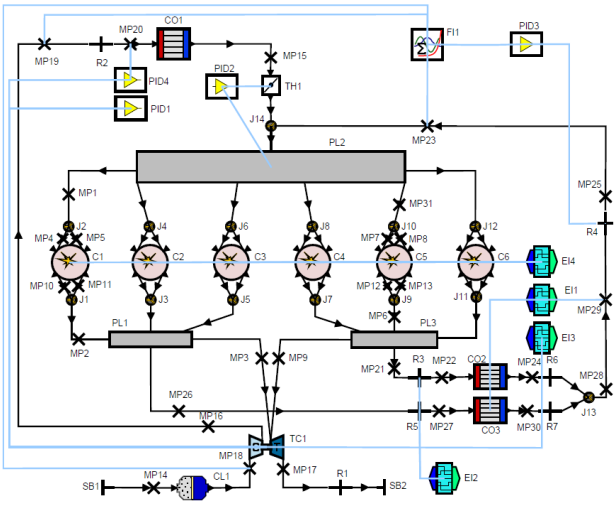

Figure 11 Simulation model of the HDGAS engine [13]

The 1D engine simulations were performed at the beginning of the project to define the thermodynamic layout of the HDGAS engine. This included valve timing, so different concepts for the gas exchange, like Early and Late Miller timing, were evaluated. Moreover, the turbocharger matching and the definition of the EGR layout were performed: for these purposes, a 1D simulation model was created with AVL BOOST v2013.2 software. Model calibration is an essential part of 1D engine simulations and, since at the time of the simulations the HDGAS engine did not exist, the model was calibrated and validated against measured data of an existing FPT NG engine. Later the model was adapted to the requirements of the HDGAS engine (**Figure 11**).

EGR in Stoichiometric SI Natural Gas Engines

With the introduction of the EURO VI emission legislation, the operating mode of natural gas positive ignition engines was shifted from lean towards stoichiometric operation. Thereby, a three way catalyst can be used to comply with the very stringent emission limits. However, stoichiometric operation entails negative effects on the fuel efficiency and the thermal strain of the engine. EGR has received attention for the application in NG positive ignition engines to mitigate these penalties **[14][15]**, due to its multiple effects.

Recirculated exhaust gas dilutes the fresh charge, increasing the inert mass in the combustion chamber and lowering the combustion temperature: as a consequence, also the exhaust gas temperature is reduced, and this lessens the thermal stress on several engine components, especially at the turbine inlet, which is critical at full load operation. The reduction of combustion temperature leads to a decrease of wall-heat losses and this increases fuel efficiency. In addition, cooled EGR reduces the knocking probability: thereby, the compression ratio of the engine can be raised and the combustion can be advanced to increase efficiency. Furthermore, the caloric properties of the charge during compression are altered: the isentropic exponent and the compression work is reduced, and fuel efficiency benefits from this.

Finally, the intake manifold pressure must be raised, when EGR is added, to maintain the load. In partial load operation this results in de-throttling and a reduction of the gas exchange losses. Also at full load operation the gas exchange losses can be reduced in combination with a waste gate turbocharger. The higher boost pressure leads to closing of the waste gate and, because of EGR, the turbocharger operates in an area of better efficiency

A trade-off exists between the gas exchange losses and the achievable EGR rate, for a given EGR layout. A positive pressure gradient between exhaust manifold and intake manifold is required to recirculate exhaust gas. The higher the amount of EGR, the higher the required pressure gradient and thus the higher the gas exchange losses. Several EGR layouts were evaluated to minimize the pressure losses over the EGR duct and thus limit the required pressure gradient: **Figure 12** shows the chosen configuration which outperforms the other variants investigated and is the only one capable of getting close to the EGR target curve, defined for each

engine speed at full load operation (curve **d** in **Figure 13**).

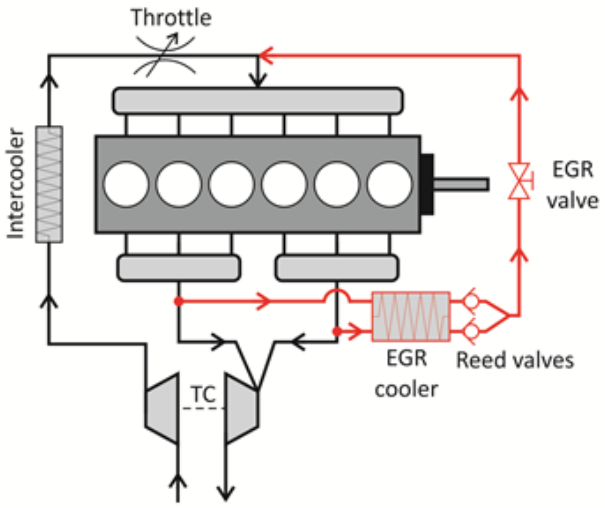

Figure 12 The chosen EGR layout [13]

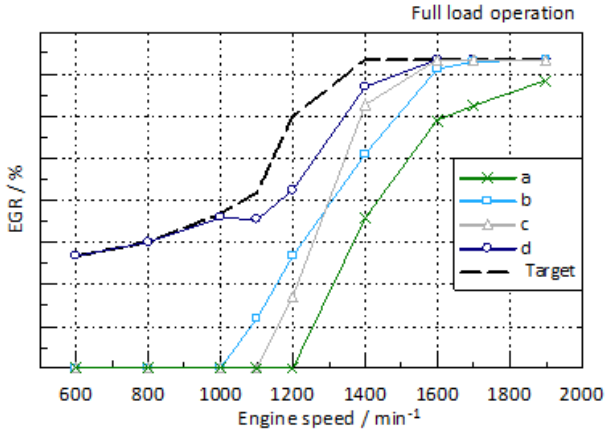

Figure 13 Calculated EGR rate with different layouts vs. target [13]

The Effects of EGR at Partial Load

The simulations results with and without EGR are shown in **Figure 14Fehler! Verweisquelle konnte nicht gefunden werden.** to quantify the effects of EGR. The part load operation point at 1200 rpm and 8 bar BMEP is chosen for this comparison. In this condition the engine is throttled and, with EGR, the intake manifold pressure must be raised by 200 mbar in order to maintain the load. The exhaust manifold pressure remains almost unchanged, consequently the gas exchange losses decrease by 200 mbar. The reduction of the combustion temperature is observed in the wall heat losses (-13%) and the exhaust gas temperature (-120 degC). The reduction of the wall heat losses and the change in the caloric properties of the cylinder charge cumulate and increase the gross indicated efficiency by 1.2%Pt. The sum of all described effects results in a rise of the net indicated efficiency, by 1.9%Pt. **[13].** These results clearly demonstrate the positive effect of EGR on fuel efficiency and thermal stress of natural gas positive ignition engines and confirm the results published in literature.

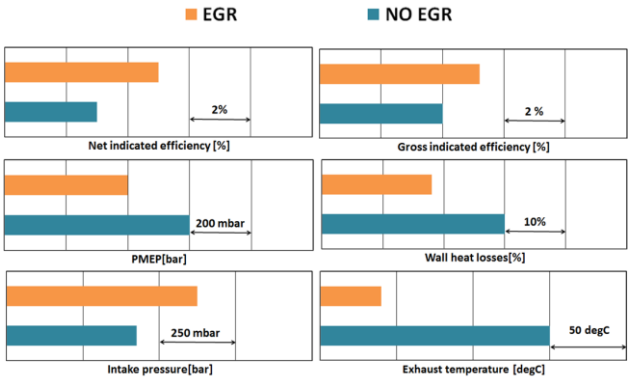

Figure 14 The effects of EGR at partial load operation [13]

Early and Late Miller Valve Timing

Apart from conventional valve timing, which is optimised for maximum volumetric efficiency, the Early and Late Miller (a.k.a. Atkinson) cycle were investigated: they are characterised by an early, and, respectively late intake valve closing (IVC) while, from a thermodynamic point of view, the processes are identical.

Compared to a conventional valve timing, the early IVC allows overexpansion of the fresh charge, which is then compressed again but the compression above intake conditions only starts when the piston again reaches the position it had at IVC: this reduces the volumetric efficiency, de-throttling the engine and decreasing gas exchange work.

Charge temperature undergoes the same changes, therefore it is lower, at a given crank angle, compared to standard valve timing: this beneficially affects the conflict between knock, compression ratio and maximum attainable load **[13]**.

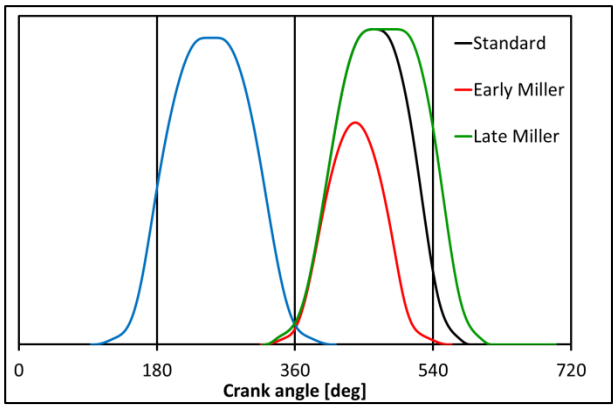

Figure 15 Valve lift profiles

The described effects, valid for Early Miller timing, also apply to Late Miller timing.

Figure 15 shows the intake and exhaust valve lift profiles used for the simulations.

The effects of early and late Miller in rated power conditions (1900 rpm-370 kW) are shown in **Figure 17**: keeping the temperature at the intercooler outlet constant, the in-cylinder temperature at firing with "Early Miller" profile is between around 30 degC lower than with the standard profile, while with "Late Miller" profile the reduction is around 10 degC **[13]**.

The intake manifold pressure must be raised by more than 500mbar with "Early Miller" timing and by 300mbar with "Late Miller" timing. Contrary to the EGR case, the exhaust manifold pressure also rises considerably, therefore, the reduction of the gas exchange losses is lower, always compared to the no EGR vs.EGR case.

The reason is the turbocharger efficiency, as demonstrated in **Figure 16Fehler! Verweisquelle konnte nicht gefunden werden.**: the introduction of EGR shifts the operating points of the compressor towards higher efficiency, from the black curve to blue one, so that the compressor works in optimal conditions. With both Miller timings too the compressor works close to the optimum, but the difference, compared to the EGR case, is very small, and the efficiency remains approximately constant, because the maximum has already been reached **[13]**.

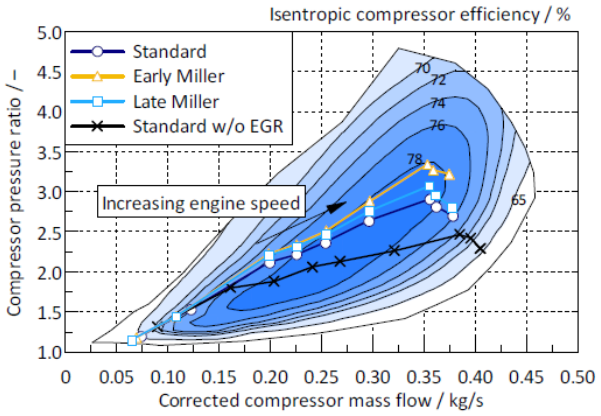

Figure 16 The compressor operating map and the operating points at full load with different valve timings [13]

The influence of Miller timing on the net indicated efficiency, which includes the positive effect on the gas exchange losses, is shown in **Figure 17**: "Early Miller" timing increases the efficiency by 0.3%$_{Pt}$ at 1900 rpm while with "Late Miller" profile the improvement is 0.1%$_{Pt}$ **[13]**.

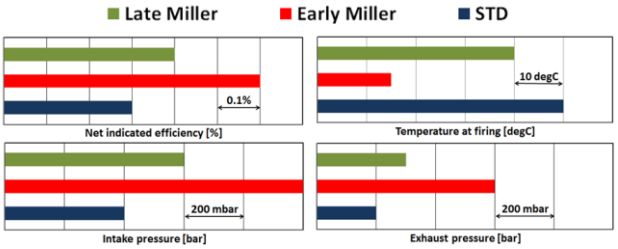

Figure 17 Effects of different valve profiles at rated power [13]

Finally, **Figure18** depicts the p-V and T-V diagrams: IVC is defined at 1 mm effective valve lift and added in the graphs. The overexpansion in the case of "Early Miller" timing, the higher intake manifold pressure and the lower charge temperature are well observed **[13]**.

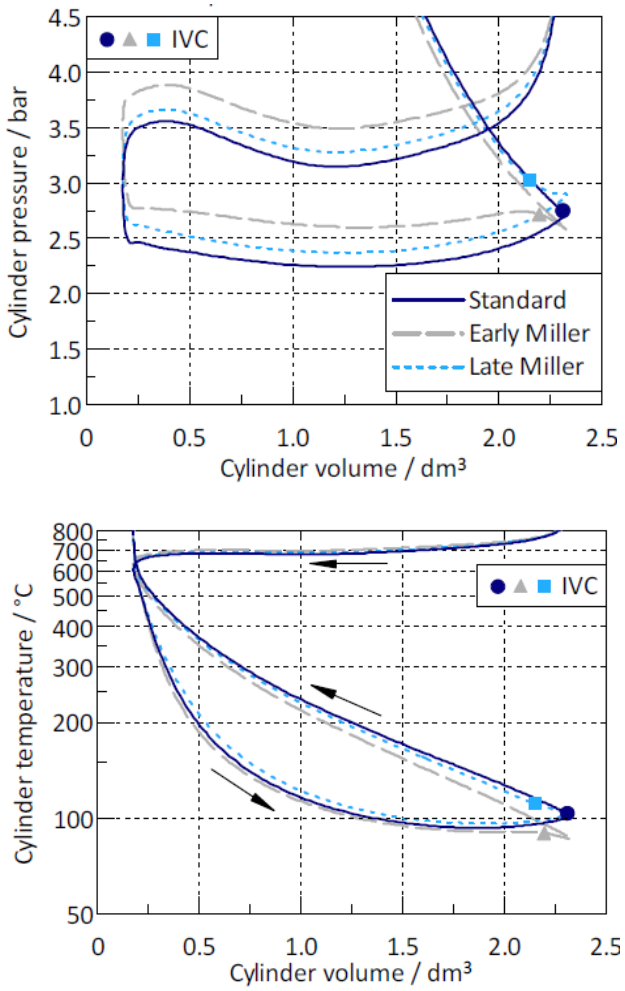

Figure 18 The p-V and T-V diagrams for Early Miller, Late Miller and standard timing [13]

CFD SIMULATIONS

CFD simulations were carried out using the open source OpenFOAM® technology coupled with the LibICE, which consists of a set of applications, solvers and libraries specifically developed during the years at the ICE Group of Politecnico di Milano. Such numerical methodology was extensively validated in previous works **[16][17][18]**. Simulations were performed using a Reynolds-averaged Navier-Stokes turbulence modelling approach.

The work activity was divided into three steps:

1. At first, steady-state flow bench simulations were performed. Different configurations of the engine intake ports were tested to find the best compromise between engine tumble intensity and flow discharge coefficient
2. Different engine operating points and valve lift profiles, at partial and full-load conditions, were tested by means of transient cold-flow, full-cycle simulations. The evolution of in-cylinder tumble motion and turbulent kinetic energy were assessed
3. Finally, fuel injection was introduced and the efficiency of the air-fuel mixing process was evaluated taking into account the homogeneity level of the mixture inside the combustion chamber. One engine operating point at partial load was tested, as well as the full-load condition with two different intake valve lift profiles.

Steady-State Flow Bench Simulations

Proper in-cylinder filling and charge flow motion intensity are fundamental to have a stable and efficient combustion process, so steady-state flow bench simulations focused on the evaluation of the Flow Coefficient (C_d) and the Tumble Ratio (TR). The former was expressed in a normalized form according to

$$c_d = \frac{\dot{m}}{\dot{m_{th}}}$$

where $\dot{m}$ is the measured mass flow rate while $\dot{m}_{th}$ is the maximum theoretical mass flow rate defined as

$$\dot{m_{th}} = Z\frac{d_v^2\pi}{4}\rho\sqrt{\frac{2\Delta p}{\rho_m}}$$

where:

Z	Number of valves
d_v	Valve inner seat diameter
Δp	Pressure drop across the valve
ρ	Air density

TR was defined as

$$TR = \frac{\omega_{FK}}{\omega_{Mot}}$$

where ω_{FK} and ω_{Mot} are respectively the angular velocity of solid body rotation and the engine angular speed.

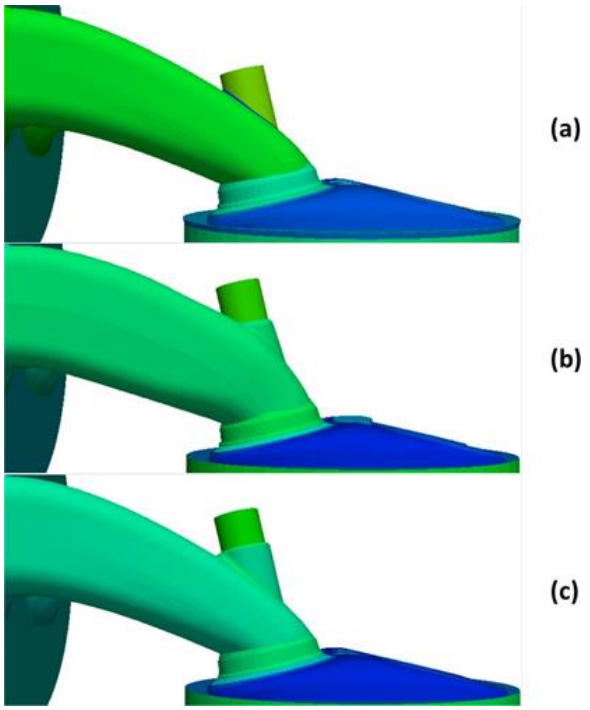

Figure 19 Evolution of intake ports layout [19]

Figure 19 Fehler! Verweisquelle konnte nicht gefunden werden. reports the three different ports layouts tested under steady-state flow bench conditions. Layout (a) represents the initial geometry, while (b) and (c) represent the modifications which were carried out on the basis of the results of CFD simulations. Layout (b) is characterized by a larger section aimed at enhancing the mass flow rate. Layout (c) displays intake ducts which are more oriented towards the opposite cylinder wall, similar to geometry (a), but with an increase of the flow cross sectional area close to the caps of the valves stems.

Overall, **Figure 20** demonstrates the capability of layout (c) to provide a good compromise between the discharge flow coefficient and the tumble motion intensity so this configuration was employed for further simulations and was used for the cylinder head casting.

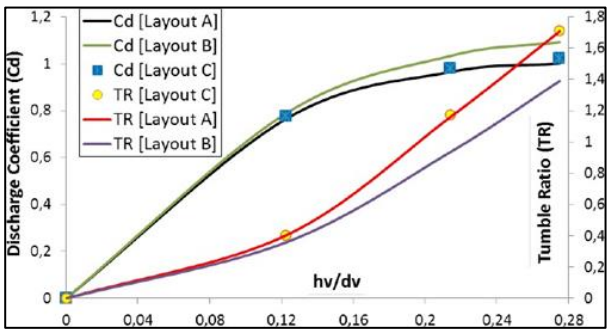

Figure 20 TR and Cd for the different layouts of the intake ducts [19]

Full-Cycle Cold-Flow Simulations

Once the geometry of the intake ports was defined, the second step was the simulation of the flow field in the cylinder with moving boundaries, during a whole working cycle, not taking into account fuel injection and combustion.

The aim of this simulation is the analysis of the flow motion evolution during intake and compression strokes in order to determine the conditions (mainly turbulence level, to guarantee a complete and fast combustion) in the proximity of the igniter at ignition timing.

The operating condition which were analysed are listed below.

Full load	370 kW @ 1900 rpm
Full torque	2200 Nm @ 1000 rpm
Partial load	100 kW @ 1200 rpm

Calculations were started at 335 deg CA with a timestep of 0.005 deg CA.

Boundary conditions derived from 1D analysis were imposed. The in-cylinder TR was evaluated according to the methodology proposed in [20].

Valve lift profiles are shown in **Figure 15**.

Figure 21 displays the TR trend for the full-load operating condition with the “Early Miller”.profile.

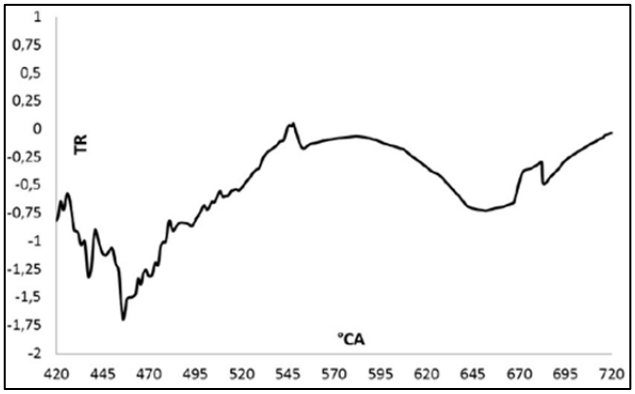

Figure 21 TR evolution: full-load [19]

The shape of the curve is consistent with what was achieved in previous full-cycle simulations of DI engines **[21],** with a peak during the intake phase, a decrease and then a lower peak before the end of the compression phase.

It was then decided to compare the evolution of the turbulence level for different intake valve lift profiles.

Figure 22 shows the result for "Early Miller" vs. "Late Miller" profile: it is quite evident that the "Late Miller" profile exhibits a higher level of turbulence (i.e. TKE) during the last phase of the compression stroke, and this should guarantee a faster flame propagation, which will result in higher engine efficiency. The difference arises because, with the "Early Mller" profile, the lower valve lift combines with the early IVC to destroy quite quickly the big-scale structures: as a consequence, this leads to a turbulence decay in the first part of the compression stroke. With the other two profiles, and especially in the "Late Miller" case, the intake valves remain at the maximum lift (which is considerably higher than in the "Early Miller" profile) for a long interval: the result is a macro-vortex which remains basically unchanged during the piston descent and which is "compressed" when the piston moves toward TDC, so that the macro-scale vortex is converted to small-scale turbulence, as demonstrated by the second peak in **Figure 22Fehler! Verweisquelle konnte nicht gefunden werden.**. Contrary to what was found in the 1D analysis, the "Early Miller" timing seems to negatively affect the combustion process compared to the Standard or the "Late Miller" profile.

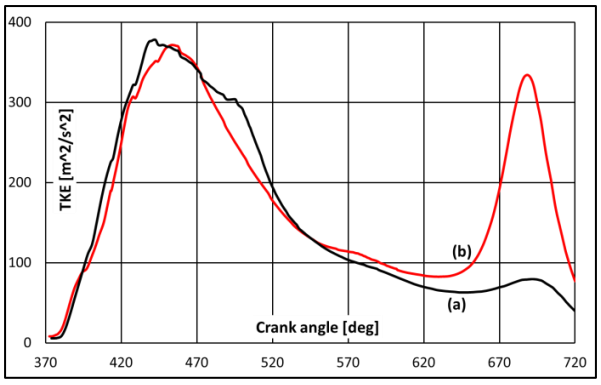

Figure 22 TKE evolution for two different valve lift profiles, full load : (a) "Early Miller", (b) "Late Miller" [19]

Full-Cycle Simulations with Natural Gas Injection

The influence of gas injection on the efficiency of the air-fuel mixing process was then evaluated.

Different engine operating conditions were considered and multiple valve lift profiles were used to verify the effects on mixing. The conditions simulated were:

1. 1300 rpm, 2 bar BMEP with "Early Miller" profile
2. Full-load with "Early Miller" profile
3. Full-load with "Late Miller" profile.

Natural gas with a volume fraction of 84.7% in methane was injected through a centrally mounted, multi-hole, direct injector with a pressure of approximately 20 bar.

The different SOI timings used are listed below

1300 rpm-2 bar	424 deg CA
	444 deg CA
Full load (both profiles)	413 deg CA

The computational mesh was refined to better capture the complex phenomena occurring during the injection phase and its interaction with the air flow.

The efficiency of the air-fuel mixing process was evaluated in terms of:

- Relative air-fuel ratio *Lambda*, defined as

$$Lambda = \frac{\left(\frac{m_{air}}{m_{fuel}}\right)}{\left(\frac{m_{air}}{m_{fuel}}\right)|_{Stoichiometric}}$$

  Since each case was simulated under stoichiometric conditions, Lambda was always expected to be unitary at the end of compression stroke. The stoichiometric air-fuel ratio of the natural gas composition used is 15.46.

- The *Homogeneity Index* (HI), which accounts for local distribution of the fuel (=1 in case of ideal homogeneous distribution)

The evolution of HI for the "1300 rpm-2 bar" case is reported in **Figure 23**Fehler! Verweisquelle konnte nicht gefunden werden.: the air-fuel homogeneity gradually increases during the injection phase, almost reaching a unitary value at the end of the compression stroke and this trend is consistent with what was observed in previous works **[21]**

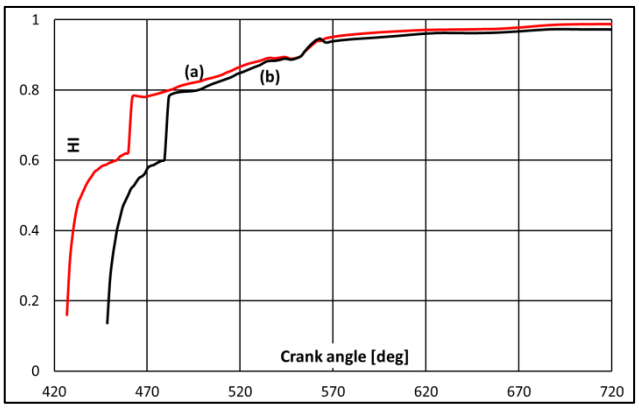

Figure 23 HI evolution for “1300rpm-2bar”: (a) SOI=424 deg, (b) SOI=444 deg [19]

Figure 23 also demonstrates that there is very little difference between the two different SOI, even though the case with earlier SOI shows a slightly higher HI at the end of the compression stroke, because of the longer time available for mixing.

Figure 24 shows the probability mass function (PMF) of Lambda, calculated for the “Late Miller” case at 720 deg CA: as expected for a stoichiometric condition, most of the mixture is characterized by a lambda value close to one, thus ensuring a stable combustion process even in full load.

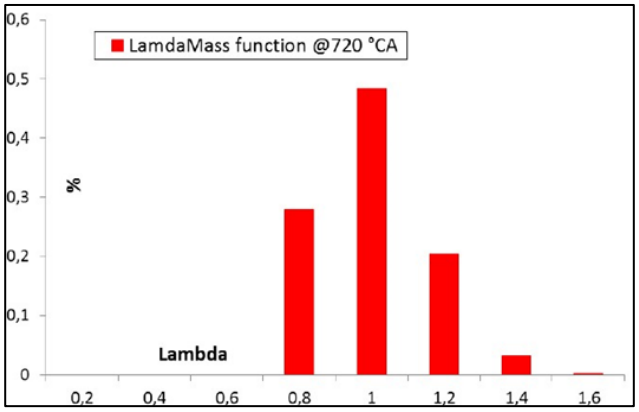

Figure 24 In-cylinder lambda distribution at 720 deg CA; full load, “Late Miller” profile [19]

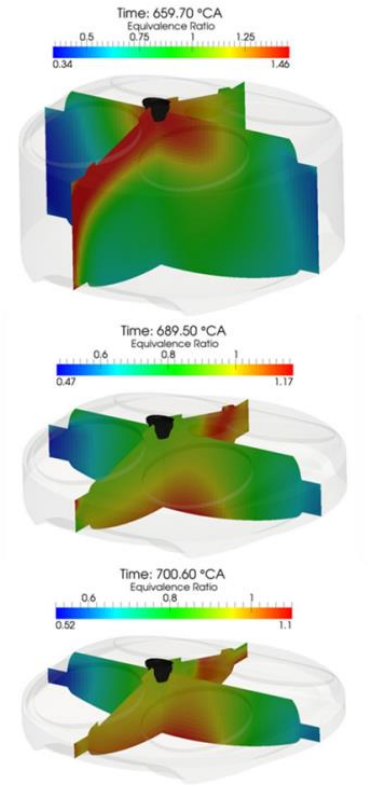

Figure 25 Distribution of in-cylinder equivalence ratio during the compression stroke; full load, “Late Miller” profile [19].

Finally, **Figure 25** reports the distribution of in-cylinder equivalence ratio (i.e. 1/ *lambda*) for the full load simulation with “Late Miller” profile on two orthogonal planes during the compression stroke. An almost homogeneous mixture (equivalence ratio equal to 1) is found close to the ignition location, thus increasing the efficiency of the ignition process, though it is possible to discriminate lean zones, close to the cylinder liner, and rich zones close to the piston: the first ones might lead to HC formation while the second ones can lead to CO generation. However, the computed high levels of in-cylinder turbulence are expected to enhance the mixing during combustion

SINGLE-CYLINDER ENGINE TESTING

The single cylinder research engine was operated on an AVL test bed in Graz, Austria where the evaluation of different camshaft profiles, injector configurations, cooled EGR and the combustion chamber itself was performed.

The main advantages of single cylinder engines are lower costs for prototype hardware and lower assembly time for hardware change on the test bed. Since single cylinder engines are externally charged, they provide a degree of freedom in setting the operation points, like boost pressure and exhaust back pressure.

For the investigation of the stoichiometric concept, it brought the following particular benefits:

- Operation with rapid prototype engine control unit possible
- One instead of six cylinders brings a cost reduction, since fewer cost-intensive prototype parts are necessary
- Drift or malfunction on prototype parts are relatively easy to detect
- The operation of the engine is independent from turbocharger hardware (freedom in boost pressure and EGR rate). This gives more liberty to investigate combustion parameters and its sensitivity to them
- Parameters can be investigated independently. Lambda independent from gas exchange work, independent from MFB50.

Characteristics of the single cylinder research engine, based on the HDGAS engine (**Figure 26**) are:

- Bore x Stroke=135 x 150 mm
- Swept volume= 2.1 dm^3

- AVL Rapid Prototype Engine Management System for closed loop AFR control
- Gas injector designed for high injection pressure
- Cylinder head for single cylinder operation with innovative charge motion
- Boost pressure control by an external supply
- Back pressure control by an electrically-actuated back pressure valve

Figure 26 AVL SCE, based on the HDGAS engine [22]

Potential of cooled EGR

MFB50-EGR variations on a single cylinder engine can show whether desired EGR rates can be applied for multi-cylinder engine applications. The maximum EGR rate is usually limited by misfire, HC emissions or instability in combustion (COV).

Figure 27 shows the influence of MFB50 and EGR rate on brake thermal efficiency, delta pressure over the engine, CH_4 emissions and COV for the partial load point (1200 rpm-8 bar BMEP).

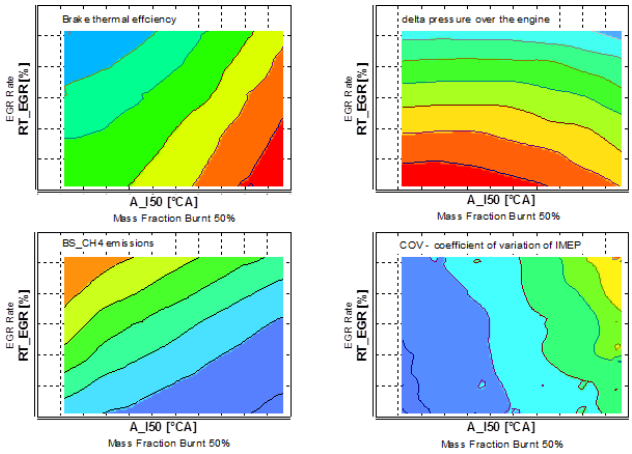

Figure 27 Influence of EGR on different parameters in partial load [22]

Figure 28 shows ignition timing variations for different EGR rates in partial load conditions: increase in the EGR rate leads to increase in brake thermal efficiency of the engine. For a constant lambda set point, more EGR reduces CO emission while CH_4 increases.

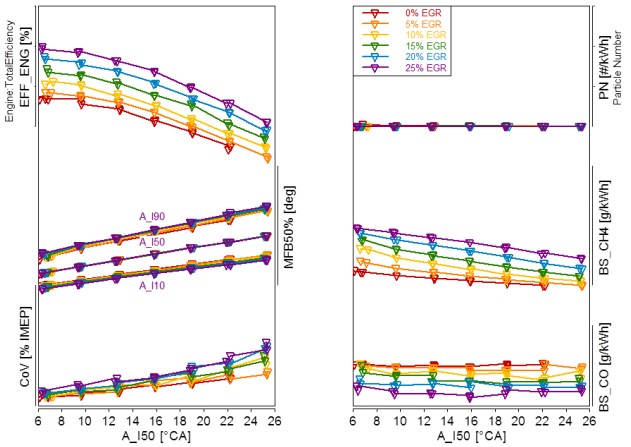

Figure 28 Influence of EGR on different parameters in partial load [22]

Figure 28 also shows that combustion duration (measured as A_I90 minus A_I10) increases with the percentage of EGR. And cycle to cycle variation increases too while the rate of heat release is stretched (**Figure 29** and **Figure 30**): nonetheless, these negative effects are outweighed by the positive ones: reduced wall-heat losses and reduced scavenging work. Furthermore, in full load conditions EGR can help reduce knocking, allowing advanced spark timing and improving fuel efficiency.

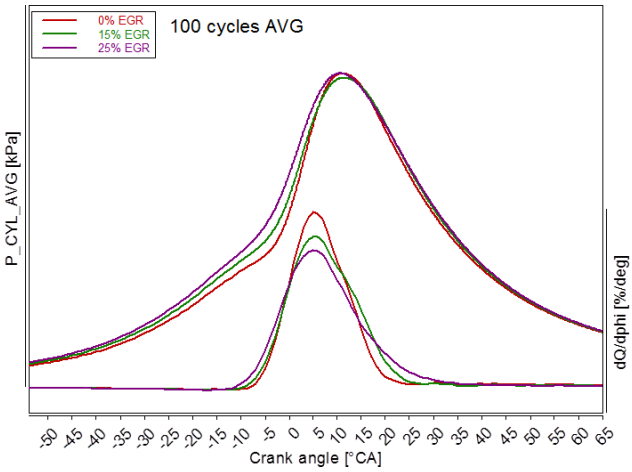

Figure 29 In-cylinder pressure and rate of heat release for different EGR rates in partial load (average cycle) [22]

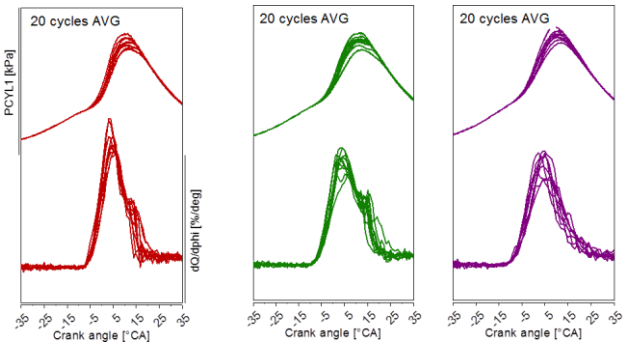

Figure 30 In-cylinder pressure and rate of heat release for different EGR rates in partial load [22]

Investigations of alternative camshaft profiles

As we have seen, three different intake valve camshafts were foreseen during the SCE test campaign. A volumetric efficiency optimized intake valve timing, which was basically a carry-over from the standard diesel application, as well as two Miller camshafts: the design target for both Miller timings was the same volumetric efficiency at low engine revs, in order to guarantee the same low-end torque (**Figure 15**).

Figure 31 shows in-cylinder pressure and rate of heat release from SCE operation for the three different camshafts.

Indeed, combustion with the “Early Miller” profile results in a significantly slower turbulent flame velocity and therefore longer heat release. Important for this comparison: all different valve lift curves were evaluated using the same intake port design.

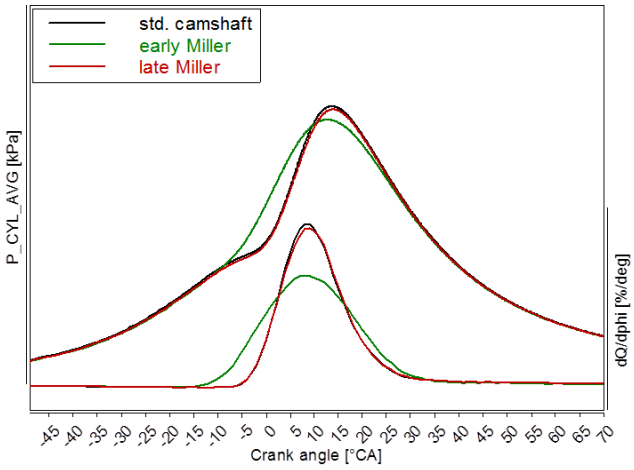

Figure 31 In-cylinder pressure and rate of heat release for different intake profiles in full torque (average cycle)

On the SCE, the effects of the different evolution of turbulence highlighted by CFD (**Figure 22Fehler! Verweisquelle konnte nicht gefunden werden.**) are clearly visible on the combustion process and offset the thermodynamic advantages shown by 1D analysis which, due to its intrinsic limitation, is not able to capture the flow evolution in the combustion chamber.

All in all, the thermodynamic benefit of a late IVC can be utilized without major changes of the combustion concept. Achieving similar thermodynamic benefits with an early IVC requires a careful adaptation of charge motion to avoid disadvantages in the combustion process.

MULTI-CYLINDER ENGINE TESTING

The multi-cylinder prototype engine was assembled in proto workshop in the FPT’s plant in Bourbon Lancy (France) and it was then delivered to FPT’s testing facilities in Foggia (Italy), where it was installed on a dynamic test bench.

A complete overhaul of the control system had been going on in parallel to the design and assembly of the prototype, due to the new content of the engine. The new injection and ignition systems, the VVT and the EGR valve, all required modification to the existing control system: a new HW ECU was necessary to manage the new components and an auxiliary Smart Driver Unit was introduced to control the injectors, which needed 65V to operate correctly. From the SW point of view, new control strategies were created.

Experimental set-up

The HDGAS engine was installed on a dynamic test bench, able to simulate also motoring conditions, featuring a 450 kW/3500 Nm dynamometer.

This test bed is normally used for development purposes and it is certified according to Accredia; it is equipped with the following instrumentation:

- ABB sensyflow FMT700-P to measure air flow
- Micro motion CMF025 to measure fuel flow
- AVL AMAi60SII-R2C-EGR analyser to measure CO, THC, O_2, CH_4, CO_2
- AVL LDD analyser to measure NO, N_2O, H_2O, NH_3
- AVL 489 to measure PN
- AVL Indimodul for in-cylinder pressure (6 channels)
- Eurins AdaMo control system to manage the test bench.

Following FPT's best practice, prior to the proto assembly, the cylinder head was machined to install one pressure sensor in each cylinder, to monitor the combustion process, and a total of 8 thermocouples, to keep the thermal condition of the head under control: moreover, upon the installation on test bench, the whole engine was instrumented in order to completely monitor the various parameters during the testing.

Engine testing

The first operation performed on the engine was the debug of the new components and systems as well as the control system, both HW and SW and, once this operation was successfully completed, the engine was run-in.

Following this, it was possible to test the maximum performance of the engine. The goal of the project was to improve by 10% power and torque compared to the 2013 state-of-the-art NG engines which translated in 2200 Nm and 370 kW, target that was reached, as it is shown in **Figure 32**.

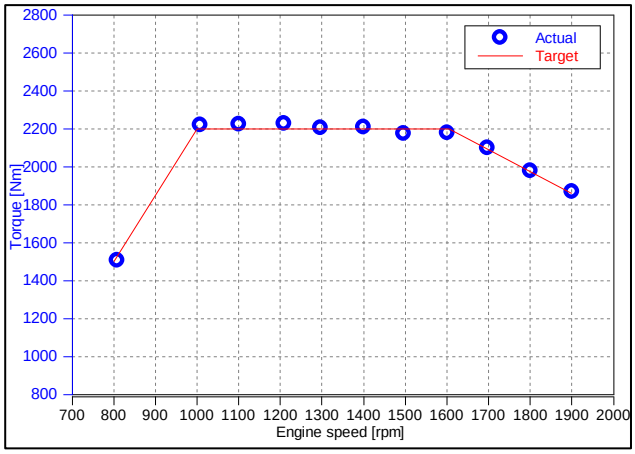

Figure 32 HDGAS performance, target vs. actual

As mentioned in the CFD section, calculations showed that, with the "Early Miller" profile, turbulence is less favourable, compared to the "Standard" profile, thus worsening engine's performance: this was confirmed during the tests with the SCE, even though the difference was not so huge.

It was decided to test the "Early Miller" profile also on the MCE, to further verify the results of CFD and SCE: as **Figure 33** shows, fuel consumption with "Standard" profile is significantly better than fuel consumption with "Early Miller" profile ("Hard Miller" in the figure), with an improvement of around 4% all over the full load curve (area A). It was therefore decided to continue testing using the "Standard" profile only.

Figure 33 also shows the fuel consumption curve for the "Standard" profile with the addition of EGR: in this case, fuel consumption is further reduced, as predicted by 1D simulations and confirmed by SCE testing (Area B). On the overall, the best configuration ("Standard" profile with EGR) gives an advantage in fuel consumption ranging between 5 and 8% on the full load curve if compared to "Early Miller" profile without EGR.

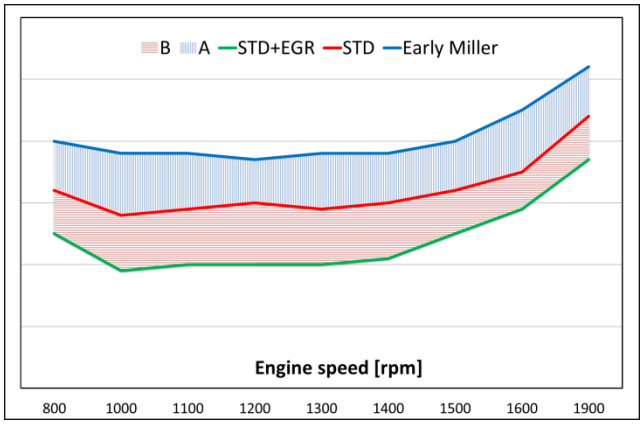

Figure 33 Fuel consumption in different engine configurations

The optimization process of the engine in steady state conditions followed: this process is aimed at finding the combination of the various factors that affect the engine's performance (ignition timing, injection phasing, air control through throttle valve and WG, EGR valve opening) in order to identify the conditions that enable to achieve the optimum in terms of fuel consumption, combustion stability, margin vs. knock and emissions.

The analysis was conducted over the same four operative points tested by AVL on the SCE:

- Operating Point 1 (1200 rpm-8 bar BMEP)
- Operating Point 2 (1000 rpm-2200 Nm)

- Operating Point 3 (1200 rpm-2200 Nm)
- Operating Point 4 (1900 rpm-370 kW)

The experiment was designed to check, at first, the effect of each single innovative technology, then the combined effects of the various technologies employed.

First of all, EOI sweep was performed. The use of Direct Injection involves restrictions on the injection phase, namely:

- Injection must start after EVC, to avoid fuel short circuit to the exhaust
- Injection may not be delayed indefinitely, to prevent subsonic flow through the injector.

The consequence of these constraints is a limitation in the maximum duration of injection.

Retarding EOI leads to a faster combustion, as reported in which shows how MBF50 is anticipated with delayed EOI.

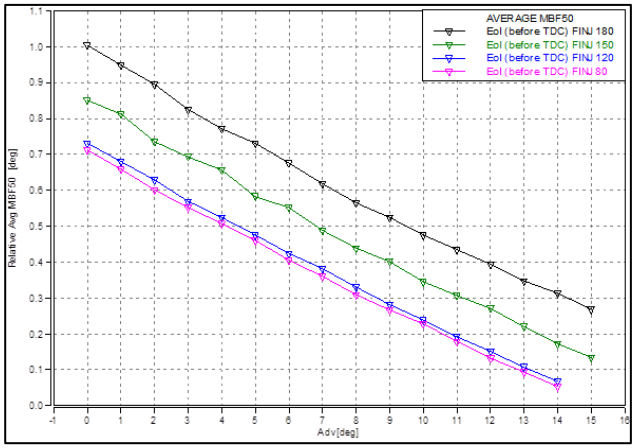

Figure 34 MBF 50 (average over 6 cylinders) vs. EOI

Then, with the optimum EOI, spark advance sweep was carried out: starting from very retarded spark timing (IMEP covariance around 6), spark timing was advanced to reach the Knock Limiting Spark Advance (KLSA). Finally, sweeps of the Corona system parameters (first ignition voltage and then duration) was performed. **Figure 35** shows the effect of the spark sweep on fuel consumption at Operating Point 1 with minimum BSFC reached at 8 deg CA after TDC.

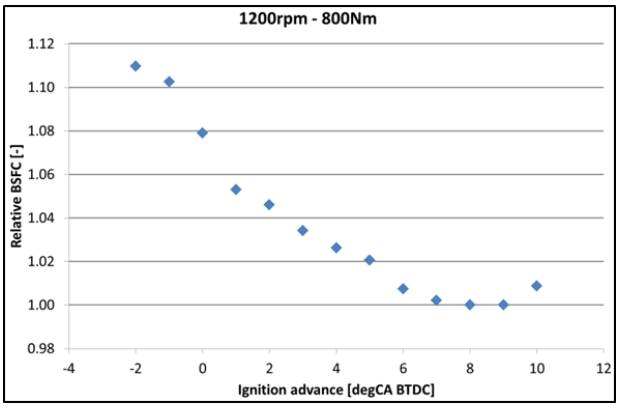

Figure 35 Spark timing effect on BSFC, Operating Point 1

Engine optimization led to excellent BSFC values in the whole map, with efficiency exceeding 40% in various operating conditions.

At the end of the project, the engine was capable of performing a complete WHTC, in order demonstrate a 10% CO_2 reduction on hot WHTC vs. 2013 state-of-the-art engine: the engine reached a 12% reduction in CO_2 emission, therefore exceeding the target. Compared to a more up-to-date gas engine as the Cursor13 NG, the HDGAS engine showed a 4% improvement in fuel consumption over the same WHTC.

CONCLUSIONS

Natural gas engines can help reach the target for CO_2 reduction, especially when used with bio-methane; moreover, they are readily available and their diffusion is growing, mainly in long haul missions.

In order to improve the thermal efficiency of gas engines (and, thus, further reduce GHG emissions), FPT joined the HDGAS project, to design and test an innovative engine, specifically conceived to work witn natural gas, and incorporating several advanced features, many of which used for the first time on an HD engine.

Working in close cooperation with other Partners (AVL, Politecnico di Milano and TUG), the task was accomplished employing advanced state-of-the-art 1D and CFD calculations to complement the design, and SCE testing to confirm calculation results: the outcome is an engine which reached the project's targets, showing a significant reduction in fuel consumption compared to the best natural gas engine currently available.

ACKNOWLEDGMENTS

The Authors would like to thank the other Partners of WP4 of the HDGAS project for their support.

The research leading to these results received funding from the European Community's Horizon 2020 Program under grant agreement 653391 (HDGAS PROJECT).

REFERENCES

[1] Ellingsen, L. A-W., Hung, C. R., *Research for TRAN Committee – Resources, energy, and lifecycle greenhouse gas emission aspects of electric vehicles*, European Parliament, Policy Department for Structural and Cohesion Policies, Brussels, 2018, doi: 10.2861/944056 – Internet http://bit.ly/2HDKk0y

[2] IEA (International Energy Agency), *The Future of Trucks: Implications for energy and the environment*, 2017

[3] Möhring L., Andersen J.: "CNG Mobility – Scalable, Affordable and Readily Available Solution for Environmental and Climate Challenges", *38th Internationales Wiener Motorensymposium*, Wien, 2017

[4] RICARDO, *Impact Analysis of Mass EV Adoption and Low Carbon Intensity Fuels Scenarios*, report on behalf of CONCAWE, 2108

[5] https://ec.europa.eu/eurostat/statistics-explained/index.php/Electricity_generation_statistics_%E2%80%93_first_results

[6] CARB (California Environmental Protection Agency Air Resource Board), *Joint agency staff report on Assembly Bill 8: 2016 assessment of time and cost needed to attain 100 hydrogen refueling stations in California*, 2017 – Internet https://www.energy.ca.gov/2017publications/CEC-600-2017-002/CEC-600-2017-002.pdf

[7] https://www.acea.be/press-releases/article/truck-co2-targets-no-public-charging-points-for-electric-or-hydrogen-trucks

[8] Semin R., "A Technical Review of Compressed Natural Gas as an Alternative Fuel for Internal Combustion Engines", American J. of Engineering and Applied Sciences 1 (4): 302-311, 2008

[9] Schuller O. et al., *Greenhouse Gas Intensity of Natural Gas*, Thinkstep report on behalf of NGVA Europe, 2017

[10] http://www.ansa.it/canale_motori/notizie/eco_mobilita/2018/10/25/iveco-stralis-a-metano-da-record-1.728-km-con-un-pieno_1217b6ee-8fcd-4087-8804-ac31f3f3cfd2.html

[11] Krähenbühl P. et al., "FPT Industrial's Leadership in Natural Gas Technologies for Industrial Engines", *38th Internationales Wiener Motorensymposium*, Wien, 2017

[12] Heywood J. B., *Internal Combustion Engine Fundamentals*, McGraw Hill Inc., New York, 1988

[13] Fasching P., *Natural Gas as Fuel for Monovalent and Dual Fuel Combustion Engines - an Experimental and Numerical Study*, Ph.D. thesis, Technische Universität Graz, Graz, 2017

[14] Figer, G et al., "Nutzfahrzeug-Gasmotoren mit Dieseleffizienz", MTZ – Motortechnische Zeitschrift, 75, (10), 2014, doi:10.1007/s35146-014-0573-4

[15] Geiger, J. et al., "Der Erdgasmotor als Nutzfahrzeugantrieb – Trends und Herausforderungen bei der Entwicklung", *8th Conference on Gas-Powered Vehicles*, Stuttgart, 2013

[16] Lucchini T. et al., "Multi-dimensional modelling of the air/fuel mixture formation process in a PFI engine for motorcycle applications," SAE Technical Paper 2009-24-0015, 2009, doi: 10.4271/2009-240015

[17] Montanaro A. et al., "Experimental Characterization of High-Pressure Impinging Sprays for CFD Modelling of GDI Engines," *SAE Int. J. Engines* 4 (1):747-763, 2011, doi: 10.4271/2011-01-0685

[18] Lucchini T. et al., "Automatic Mesh Generation for CFD Simulations of Direct-Injection Engines," SAE Technical Paper 2015-01-0376, 2015, doi: 10.4271/2015-01-0376

[19] Paredi D. et al., "Gas Exchange and Injection Modelling of an Advanced Natural Gas Engine for Heavy Duty Applications," SAE Technical Paper 2017-24-0026, 2017, doi: 10.4271/2017-24-0026

[20] Scarcelli R. et al., "CFD and optical investigations of fluid dynamics and mixture formation in a DI-H_2 ICE" ASME, ICEF2010-35084, 2010

[21] Lucchini T. et al., "Full-Cycle CFD Modelling of Air/Fuel Mixing Process in an Optically Accessible GDI Engine," *SAE Int. J. Engines* 6(3):1610-1625, 2013, doi: 10.4271/2013-24-0024

[22] Golini S. et al., "Natural Gas Engines for Long-Haulage Applications: Current Approach and Future Developments", *16th Conference: The Working Process of the Internal Combustion Engine*, Graz, 2017

DEFINITIONS, ACRONYMS, ABBREVIATIONS

AFR	Air/Fuel Ratio
ATS	After-Treatment System
BDC	Bottom Dead Centre
BEV	Battery Electtric Vehicle
BMEP	Brake Mean Effective Pressure
CA	Crank Angle
CFD	Computational Fluid Dynamics
CNG	Compressed Natural Gas
DI	Direct Injection
EGR	Exhaust Gas Recirculation
EOI	End Of Injection
EU	European Union
FEA	Finite Element Analysis
FC	Fuel Cells
FCV	Fuel Cells Vehicle
GHG	Greenhouse Gas
HC	Unburned Hydrocarbons
HD	Heavy Duty
HDV	Heavy Duty Vehicle
HI	Homogeneity Index
HVA	Hydraulic Valve-lash Adjustement
ICE	Internal Combustion Engine
IMEP	Indicated Mean Effective Pressure
IVC	Intake Valve Closing
KLSA	Knock Limiting Spark Advance
LCV	Light Commercial Vehicles
LH	Long Haul
LNG	Liquefied Natural Gas
NG	Natural Gas
MFB	Mass Fraction Burned
MCE	Multi-Cylinder Engine
SCE	Single-Cylinder Engine
SOI	Start Of Injection
TDC	Top Dead Centre
TKE	Turbulent Kinetic Energy
TR	Tumble Ratio
WG	Wate Gate
WHTC	World Harmonised Transient Cycle